Small Molecules Showing Significant Protection of Mice against Botulinum Neurotoxin Serotype A

Yuan-Ping Pang[1]*, Jon Davis[2¤a], Shaohua Wang[1], Jewn Giew Park[1], Madhusoodana P. Nambiar[2], James J. Schmidt[3], Charles B. Millard[2]*[¤b]

1 Computer-Aided Molecular Design Laboratory, Mayo Clinic, Rochester, Minnesota, United States of America, 2 Division of Biochemistry, Walter Reed Army Institute of Research, Silver Spring, Maryland, United States of America, 3 Integrated Toxicology Division, United States Army Medical Research Institute of Infectious Diseases, Fort Detrick, Maryland, United States of America

Abstract

Botulinum neurotoxin serotype A (BoNTA) causes a life-threatening neuroparalytic disease known as botulism that could afflict large, unprotected populations if the toxin were employed in an act of bioterrorism. Current post-exposure therapy is limited to symptomatic treatment or passive immunization that is effective for treating infant botulism at a cost of US $45,300 per treatment regimen. Antibodies can neutralize the extracellular but not the intracellular BoNTA. Moreover, antibody production, storage, and administration in a mass casualty scenario pose logistical challenges. Alternatively, small-molecule inhibitors of BoNTA endopeptidase (BoNTAe) are sought to antagonize the extracellular or intracellular toxin. While several such molecules reportedly demonstrated efficacy in protecting cells against BoNTA, there is scant information to show that small molecules can significantly protect mammals against BoNTA. Herein we report the development of effective small-molecules BoNTAe inhibitors with promising *in vivo* pharmacokinetics. One such molecule has an *in vivo* half-life of 6.5 hours and is devoid of obvious sign of toxicity. Pre-treatment with this molecule at 2 mg/kg protected 100% and 70% of treated mice against BoNTA at 5 times of its median-lethal dose during the periods of 2 and 4 half-lives of the inhibitor, respectively. In contrast, 40% and 0% of untreated mice survived during the respective periods. Similar levels of protection were also observed with two other small molecules. These results demonstrate that small molecules can significantly protect mice against BoNTA and support the pursuit of small-molecule antagonists as a cost-effective alternative or as an adjunct to passive immunity for treating botulism.

Introduction

Seven distinct serotypes (A to G) of the spore-forming *Clostridium botulinum* have been characterized based upon production of structurally and functionally unique botulinum neurotoxins (BoNTs) [1]. Such toxins can cause a life-threatening neuroparalytic disease known as botulism [1] by inhibiting normal release of the neurotransmitter acetylcholine at peripheral neuromuscular junctions and thereby causing prolonged flaccid paralysis, serious medical sequelae, or death [1]. Despite its toxicity, the purified and diluted BoNT serotype A (BoNTA) can be harnessed to treat cholinergic nerve and muscle dysfunctions, as well as for cosmetic treatment of facial wrinkles [2,3]. Even in carefully controlled clinical scenarios, however, overdoses of BoNTA can occur and result in systemic botulism [4]; such incidents may rise as the number of therapeutic indications increases [5]. Mishaps also may

occur involving the use of unregulated or counterfeit formulations of BoNTA at unknown concentrations [6]. Moreover, due to its long *in vivo* half-life ($t_{1/2} > 31$ days [7]), BoNTA is a recognized biological weapon that has been sought or stockpiled by both small terrorist cells and large industrial countries [8,9]. Recently, it has been projected that botulism could afflict a large number of unprotected civilians if a food supply, for example the milk production and distribution chain [10], were intentionally contaminated by the toxin in an act of bioterrorism. There is an urgent need for small-molecule BoNTA inhibitors as effective and safe post-exposure treatment for BoNTA intoxication to respond to food poisoning, accidental clinical overdoses, and mass-casualty situations.

Current post-exposure therapy is limited to symptomatic treatment or passive immunization that is effective for treating infant botulism [11] at a cost of US $45,300 per treatment regimen

[12]. Antibodies can neutralize the extracellular but not the intracellular BoNTA. Moreover, antibody production, storage, and administration in a mass casualty scenario pose logistical challenges. To antagonize the extracellular or intracellular BoNTA, small molecules [13–20] have been developed to inhibit <u>BoNTA</u> endopeptidase (BoNTAe) – the catalytic domain of BoNTA that specifically cleaves a critical component of the neurosecretory apparatus required for acetylcholine release [21]. While several such molecules have demonstrated efficacy in protecting cells against BoNTA [13,15,20], there is scant information to show that small molecules can significantly protect mammals against BoNTA, although an *in vivo* study of small-molecule BoNTAe inhibitors has been reported [22].

Herein, we report the development of effective small-molecule BoNTAe inhibitors with *in vivo* half-live of 4–6 hours. These inhibitors showed 100% and 70% of protection of mice against BoNTA at 5 times of its median-lethal dose during the periods of 2 and 4 half-lives of the inhibitors at an inhibitor concentration of 2 mg/kg, respectively. We also discuss the prospect of small-molecule inhibitors as a cost-effective alternative or as an adjunct to passive immunity for treating botulism.

Results

Design and Synthesis

We previously reported a serotype-specific, small-molecule BoNTAe inhibitor, **H3H** (structure shown in Figure 1), which has a K_i^{app} value of 3.8 ± 0.77 µM and was resulted from our lead identification and optimization as summarized in Figure 1 [14,23]. One drawback of **H3H** is insolubility in water. In optimizing **H3H** for water solubility and higher potency in inhibiting BoNTAe, we encountered problems in derivatizing **H3H** caused by chemical instability under acidic conditions (pH<2.0) that was presumably due to the proton at position 3 of the indole ring. These problems hampered the structural modifications of **H3H** guided by insights from computer simulations or the crystal structures of inhibitor-bound BoNTAe complexes.
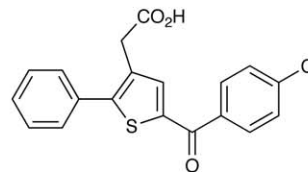
Recognizing the synthesis step as the rate-determining step of the optimization, we set out to first establish a facile synthetic scheme that can lead to a group of inhibitor analogues and then use computer simulations of the inhibitor-bound BoNTAe complexes to prioritize the syntheses of the analogues. This was different from what we did earlier, namely, first finding alternative analogues on the basis of computer simulations and then determining whether the alternatives were synthetically accessible.

Accordingly, we developed a simple synthetic scheme shown Figure 2 that begins with a known intermediate used for the synthesis of **H3H** [14]. The new scheme, which readily leads to a handful of new analogues of **H3H** by varying substituents R_1, R_2, and R_3, enabled us to address the problems of water solubility and chemical instability of **H3H** by introducing hydrophilic groups and replacing the position-3 proton of the indole ring with a fluorine atom [24], respectively. Preliminary multiple molecular dynamics simulations (10 1-ns-long simulations) suggested that two of such analogues, **F3A** and **F4H** (structures shown in Figure 1), might be able to interact favourably with the active site of BoNTAe. The simulation results were later supported by the extended multiple molecular dynamics simulations (10 10-ns-long simulations) described below.

Therefore, we made **F4H** and **F3A** with relative ease according to the scheme shown in Figure 2. Gratifyingly, we found that both **F4H** and **F3A** are water soluble at concentrations up to 5.0 mM and stable under acidic conditions.
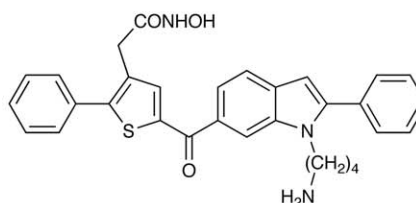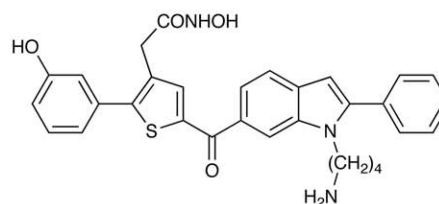
Figure 1. The development process of H3H, F4H and F3A as small-molecule BoNTAe inhibitors.
doi:10.1371/journal.pone.0010129.g001

Computer Simulation

Subsequent extended multiple molecular dynamics simulations (10 10-ns-long simulations) of BoNTAe in complex with **F4H** or **F3A** suggested that both inhibitors have (1) the hydroxamate coordinating the zinc ion embedded in the active site, (2) the hydroxamate forming a hydrogen bond to Glu224, (3) the cation-pi interaction of the thiophene-substituted phenyl group with Arg363, (4) the pi-pi interactions of the thiophene-substituted phenyl group with Phe194 and Tyr366, (5) the interaction of the ketone oxygen atom with Asp370 that is bridged by at least one

Figure 2. Synthetic scheme for F4H and F3A.
doi:10.1371/journal.pone.0010129.g002

water molecule, and (6) the cation-pi and pi-pi interactions of the indole-substituted phenyl group with Lys66 and Gln162, respectively (Figure 3). The main differences between the two inhibitor complexes are that (1) the thiophene-substituted phenyl group has stronger pi-pi interactions (judged by distance) with Tyr366 and Phe194 in **F4H•BoNTAe** than in **F3A•BoNTAe**, (2) Tyr366 forms a hydrogen bond with the carbonyl oxygen atom of the hydroxamate in **F4H•BoNTAe** but not in **F3A•BoNTAe**, and (3) the interaction between the ketone oxygen atom and Asp370 is bridged by one or two water molecules in **F4H•BoNTAe** or **F3A•BoNTAe**, respectively. The coordinates of the simulation-generated **F4H•BoNTAe** and **F3A•BoNTAe** complexes are available in Datasets S1 and S2, respectively.

Biological Evaluation

High performance liquid chromatography (HPLC)-based BoN-TAe inhibition assays [25] showed that **F4H** is as potent as **H3H** in inhibiting BoNTAe, and **F3A** is less potent than **H3H** (Table 1). Furthermore, **H3H**, **F4H**, and **F3A** showed no acute toxicity to mice. We therefore performed *in vivo* pharmacokinetic studies on all three inhibitors. Interestingly, the exposures of **F4H** and **F3A** to mice are nearly the same but slightly less than that of **H3H**, as measured by the area under the time-concentration curve (AUC), even though the maximum concentration (C_{max}) and the concentration 24 hours after one dose of a test compound (C_{24}) for each inhibitor are different (Table 1). The nearly identical half-lives ($t_{1/2} \approx 6$ hours) of **F4H** and **F3A** are longer than that of **H3H**

Figure 3. Overlay of simulation-generated models of F4H•BoNTAe (yellow) and F3A•BoNTAe (green). For clarity the water molecules that bridge the interaction between Asp370 and the ketone oxygen atom are not displayed, but these water molecules along with other active-site water molecules are included in the coordinates of Datasets S1 and S2.
doi:10.1371/journal.pone.0010129.g003

Table 1. *In Vitro* Inhibition of BoNTAe and *in Vivo* Pharmacokinetic Data for H3H, F4H, and F3A.

Inhibitor	% BoNTAe inhibition[1]	C_{max} (ng/mL)	C_{24} (ng/mL)	AUC_{last} (hr·ng/mL)	$T_{1/2}$ (hr)
H3H	78±4	497.4	3.0	1547.3	4.35
F4H	82±6	738.4	<0.5	1386.4	6.50
F3A	47±1	256.0	7.0	1385.9	6.25

[1]The inhibition assays were conducted at an inhibitor concentration of 20 µM.
doi:10.1371/journal.pone.0010129.t001

($t_{1/2} \approx 4$ hours). In this context, we further evaluated all three inhibitors using a standardized mouse model of botulism [26] to determine if they can protect mice against either extracellular or intracellular BoNTA during the period of 8 half-lives of the test inhibitor in a single-dose experiment.

Groups of Balb/c mice were given one 2-mg/kg intraperitoneal injection of **H3H**, **F4H**, **F3A**, or dimethyl sulfoxide as a control and, after 30 minutes, each mouse was challenged intraperitoneally with BoNTA at 5 times of its median-lethal dose. All mice were examined twice daily for survival, behaviour, motor activity, breath, and extraocular symptoms of botulism. Each of the three inhibitors significantly ($p < 0.05$) increased survival at different time intervals (Figure 4). Importantly, all mice treated with any of the three inhibitors survived during the 12-hour period ($\sim 2t_{1/2}$ for **F4H**) after the BoNTA challenge. During this period, the inhibitors are expected to work optimally according to the time course of the inhibitor concentration in mouse plasma. In contrast, 60% of the untreated mice died during the 12-hour period. Consistently, all untreated mice died 24 hours ($\sim 4t_{1/2}$ for **F4H**) after the challenge, whereas 70% and 60% of the **F4H**-treated mice survived 24 hours and 48 hours ($\sim 8t_{1/2}$ for **F4H**) after the challenge, respectively (Figure 4). Furthermore, 10% of the mice treated with any of the three inhibitors survived without symptoms of botulism until they were euthanized on day 5 (Figure 4).

Discussion

Small-molecule BoNTAe inhibitors have been pursued actively by different research groups [13–20], but concern remains with regard to the feasibility of the small-molecule therapy for botulism, primarily because (1) BoNTA has a long *in vivo* half-life ($t_{1/2} > 31$ days [7]), (2) small-molecule BoNTAe inhibitors with low nanomolar potencies are difficult to obtain [19], and (3) there has been only one article to date reporting an *in vivo* study of small-molecule BoNTAe inhibitors [22]. The work described above offers the following insights into the prospect of the small-molecule botulism therapy, although additional studies are needed to determine if the observed protection of mice against BoNTA by the pre-treatment of **F4H**, **H3H**, or **F3A** involves inhibition and clearance of extracellular toxin depots, uptake by intoxicated neurons, or both routes.

F4H, **H3H**, and **F3A** have *in vivo* half-lives of 4–6 hours, and all mice treated with any of the three inhibitors survived during the 12-hour period ($\sim 2t_{1/2}$ for **F4H**) after the BoNTA challenge. It is therefore plausible that the problem with a long *in vivo* half-life of BoNTA can be mitigated by treating with an **F4H**-like compound one dose per day for multiple days. This treatment could be shortened if the compound were used in combination with long-lasting antibodies [27] that are effective to neutralize the extracellular toxin.

F4H showed 82±6% inhibition of BoNTAe at the inhibitor concentration of 20 µM. However, with one 2-mg/kg intraperitoneal injection, **F4H** showed 100, 70, and 60% protection of mice against BoNTA during the 12-, 24-, and 48-hour periods after the toxin challenge, respectively. This suggests that small-molecule BoNTAe inhibitors with low nanomolar potencies might not be necessary; inhibitors with low micromolar or high nanomolar potencies may suffice.

All three different inhibitors protected 100% of treated mice during the 12-hour period ($\sim 2t_{1/2}$ for **F4H**) and 10% of the mice during the standard 5-day observation period, with a single intraperitoneal injection of the inhibitor against a supralethal BoNTA challenge. Furthermore, 90% of the **F3A**-treated mice, 40% of the **H3H**-treated mice, and 40% of the **F4H**-treated mice died 48 hours after the toxin challenge, respectively (Figure 4). The *in vivo* potencies appeared to be consistent with the *in vitro* potencies of the three inhibitors (Table 1). These results support the hypothesis that protection of mice against BoNTA can be achieved by treatment with a small-molecule BoNTAe inhibitor and are incentive to improve BoNTAe inhibitor structures and dosing regimen to optimize *in vivo* efficacies.

In summary, the present work demonstrates that small-molecule inhibitors can significantly protect mice against BoNTA and encourages the pursuit of small-molecule BoNTAe inhibitors for alternative or complementary treatment of botulism.

Materials and Methods

The animal experiments were performed with an approved protocol by the Institutional Animal Care and Use Committee at the Walter Reed Army of Institute of Research (IACUC number: B02-08) that is in compliance with the Animal Welfare Act and other United States federal statutes and regulations involving animals and adheres to principles stated in the Guide for the Care and Use of Laboratory Animals, NRC Publication, 1996 edition.

Reagents

Hexanes (Hex), ethyl acetate (EtOAc), and trifluoroacetic acid (TFA) were purchased from Fisher Scientific (Pittsburgh, PA). BSA, HEPES buffer, and zinc chloride were purchased from Sigma-Aldrich (St. Louis, MO). Dithiothreitol was obtained from BioRad (Hercules, CA). All commercially available reagents were used as received. Recombinant BoNTAe was provided by Dr. Leonard Smith of the United States Army Medical Research Institute of Infectious Diseases, Fort Detrick, MD.

Chemical Synthesis

General Description. The ^{1}H NMR (400 MHz) and ^{13}C NMR (100 MHz) spectra were recorded on a Mercury 400 spectrometer from Varian (Palo Alto, CA). Chemical shifts are
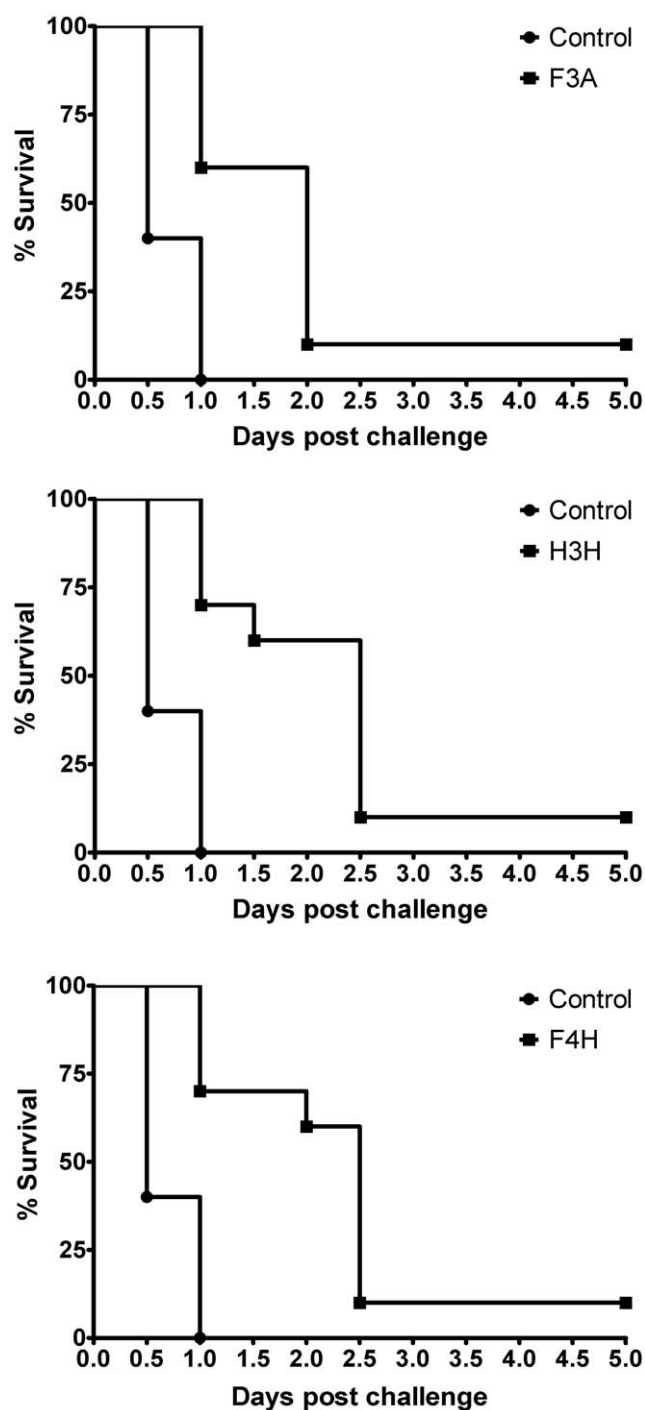
Figure 4. The survival curves of mice treated with placebo or a BoNTAe inhibitor. F3A: top, **H3H**: middle, and **F4H**: bottom.
doi:10.1371/journal.pone.0010129.g004

reported in ppm using either tetramethylsilane or the solvent peak as an internal standard. Data are reported as follows: chemical shift, multiplicity (s = singlet, brs = broad singlet, d = doublet, t = triplet, brt = broad triplet, q = quartet, m = multiplet), coupling constant, and integration. Low-resolution mass spectra were recorded using either Hewlet Packard 5973 Mass Spectrometer with SIS Direct Insertion Probe (Palo Alto, CA) or Waters ZQ/EMD 1000 Mass Spectrometer (Milford, MA). High-resolution mass spectra were obtained on a Bruker BioTOF II

ESI. IR spectra were obtained on a ThermoNicolet Avatar 370 FT-IR (Waltham, MA) using KBr pellet. Medium pressure liquid chromatography (MPLC) was performed with Biotage SP-1 (Charlottesville, VA) using silica gel (EM Science, 230–400 mesh). HPLC was carried out on a 5-µm C18 column (analytical: 4.60×250 mm, HyperClone; semi-preparative: 21.2×250 mm, Gemini) from Phenomenex (Torrance, CA) eluting with linear gradient of 80% of solution A (1000 mL of H_2O and 1 mL of TFA) to 100% of solution B (100 mL of H_2O, 900 mL of MeCN and 1 mL of TFA) over 20 minutes at a flow rate of 1.0 mL/min (analytical) or over a specified amount of time at a flow rate of 10 mL/min (semi-preparative) with UV detection at 254 nm on a Beckman Coulter System Gold HPLC system (166P detector and 125P solvent module) from Beckman Coulter (Brea, CA). KCN is highly toxic and must be handled with extreme care by trained personnel.

Methyl 2-(2-bromo-5-(1-(4-(1,3-dioxoisoindolin-2-yl)butyl)-3-fluoro-2-phenyl-1*H*-indole-6-carbonyl)thiophen-3-yl)acetate (2). To a solution of methyl 2-(2-bromo-5-(1-(4-(1,3-dioxoisoindolin-2-yl)butyl)-2-phenyl-1*H*-indole-6-carbonyl)-thiophen-3-yl)acetate (**1** in Figure 2) [14] (156 mg, 0.24 mmol) in 3 mL CH_2Cl_2 was added 1-fluoropyridinium triflate (78 mg, 0.28 mmol), and then the mixture was stirred at room temperature for 6 days. The resulting mixture was diluted with 40 mL Et_2O, washed with brine (2×10 mL), dried over $MgSO_4$, filtered, and then concentrated *in vacuo*. MPLC purification (Hex:EtOAc/9:1) gave **2** (66 mg, 41%) as a yellow solid foam. ^{1}H NMR (CDCl₃) δ 7.94 (s, 1H), 7.78−7.75 (m, 2H), 7.71−7.63 (m, 4 H), 7.57 (s, 1H), 7.50−7.39 (m, 5H), 4.25 (t, J = 7.2 Hz, 2H), 3.71 (s, 3H), 3.69 (s, 2H), 3.49 (t, J = 6.6 Hz, 2H), 1.67−1.60 (m, 2H), and 1.50−1.43 (m, 2H) (see Figure S1 for proton NMR spectrum of **2**); ^{13}C NMR (CDCl₃) δ 187.42, 170.49, 168.57, 143.91, 141.87 ($^1J_{CF}$ = 244.0 Hz), 136.06, 135.98, 135.02, 134.26, 132.30 ($^3J_{CF}$ = 7.0 Hz), 132.08, 131.54, 129.95, 129.17, 128.44 ($^3J_{CF}$ = 3.0 Hz), 127.60 ($^2J_{CF}$ = 21.0 Hz), 123.48, 122.10, 122.20, 120.17 ($^2J_{CF}$ = 16.0 Hz), 117.04 ($^3J_{CF}$ = 3.0 Hz), 112.66, 52.61 (q, J = 10.7 Hz), 43.64, 37.23, 35.07, 27.32, and 25.76; IR cm^{-1} 2921.2, 1707.6, and 1393.0; LRMS-EI m/z 672 and 674 (12% each, [M$^+$]), 160 (100%, [CH_2NPhth^+]); HRMS-ESI calculated for $C_{34}H_{26}BrFN_2O_5SNa^+$ [M+Na$^+$] 695.0622, found 695.0619.

Methyl 2-(5-(1-(4-(1,3-dioxoisoindolin-2-yl)butyl)-3-fluoro-2-phenyl-1*H*-indole-6-carbonyl)-2-(4-hydroxyphenyl)thiophen-3-yl) (3x). A mixture of **2** (42 mg, 0.062 mmol), Pd(PPh₃)₄ (8 mg, 0.007 mmol), CsF (28 mg, 0.18 mmol), 4-hydroxyphenylboronic acid (13 mg, 0.094 mmol), and H_2O (200 µL) in 1,2-dimethoxyethane (8 mL) was degassed with N₂ for 10 minutes and then refluxed for 6 hours. The resulting suspension was poured into H_2O (10 mL) and then extracted with 70 mL Et_2O. The organic layer was washed with brine (2×10 mL), dried over $MgSO_4$, and then concentrated *in vacuo*. MPLC purification (Hex:EtOAc/5:1) of the residue gave **3x** as a yellow solid foam (34 mg, 79%). ^{1}H NMR (CDCl₃) δ 7.99 (s, 1H), 7.78−7.66 (m, 7H), 7.50−7.38 (m, 7H), 6.94 (d, J = 8.4 Hz, 2H), 6.27 (s, 1H), 4.26 (t, J = 7.0 Hz, 2H), 3.69 (m, 5H), 3.48 (t, J = 6.8 Hz, 2H), 1.68−1.59 (m, 2H), and 1.50−1.43 (m, 2H) (see Figure S2 for proton NMR spectrum of **3x**); ^{13}C NMR (CDCl₃) δ 188.36, 171.87, 168.57, 157.05, 149.86, 141.93 ($^1J_{CF}$ = 244.6 Hz), 141.28, 137.87, 137.80, 134.24, 132.38, 132.35, 132.10, 131.03, 130.98 ($^3J_{CF}$ = 3.0 Hz), 129.98, 129.16, 128.56 ($^3J_{CF}$ = 3.0 Hz), 127.28 ($^2J_{CF}$ = 15.3 Hz), 125.25, 123.49, 121.42, 119.98 ($^2J_{CF}$ = 15.3 Hz), 116.93, 116.17, 112.64, 52.53 (q, J = 9.9 Hz), 43.61, 37.27, 34.49, 27.35, and 25.77; IR cm^{-1} 3391.2, 2929.4, 2851.8, 1711.7, and 1442.0; LRMS-EI m/z 687 (100%, [M$^+$]), 439 (65%); HRMS-ESI calculated for $C_{40}H_{31}FN_2O_6SNa^+$ [M+Na$^+$] 709.1779, found 709.1787.

2-(5-(1-(4-Aminobutyl)-3-fluoro-2-phenyl-1H-indole-6-car-bonyl)-2-(4-hydroxyphenyl)thiophen-3-yl)-N-hydroxyacetamide (F4H). To a stirred solution of **3x** (34 mg, 0.049 mmol) in THF/MeOH (3 mL/5 mL), 1 mL of 50% aqueous NH_2OH was added, followed by a catalytic amount (two crystals) of KCN. The resulting mixture was stirred for 23 hours at room temperature, and then filtered through a short Celite column. HPLC purification of the filtrate gave **F4H·TFA** as a yellow amorphous solid (20 mg, 60%). The semi-preparative and analytical HPLC retention times of **F4H·TFA** are 14.00 and 14.57 minutes, respectively (see Figure S3 for chromatograms of **F4H·TFA** before and after the HPLC purification). ^{1}H NMR (CD$_3$OD) δ 8.11 (s, 1H), 7.78 (s, 1H), 7.73 (d, $J = 8.4$ Hz, 1H), 7.66 (dd, $J = 1.2$, 8.4 Hz, 1H), 7.59−7.58 (m, 4H), 7.54−7.50 (m, 1H), 7.39 (d, $J = 8.6$ Hz, 2H), 6.92 (d, $J = 8.6$ Hz, 2H), 4.36 (t, $J = 7.2$ Hz, 2H), 3.51 (s, 2H), 2.79 (t, $J = 7.2$ Hz, 2H), 1.76−1.69 (m, 2H), and 1.50−1.43 (m, 2H) (see Figure S4 for proton NMR spectrum of **F4H**); ^{13}C NMR (CD$_3$OD) δ 188.80, 169.26, 160.90 (q, CF$_3$$\underline{C}O_2$H, $^2J_{CF} = 36.6$ Hz), 158.74, 150.11, 141.75 ($^1J_{CF} = 243.1$ Hz), 140.72, 137.85, 132.22, 132.15 ($^3J_{CF} = 5.3$ Hz), 130.73, 130.53, 129.85, 129.02, 128.96, 128.45 ($^3J_{CF} = 3.8$ Hz), 127.30 ($^2J_{CF} = 20.6$ Hz), 123.86, 120.58, 119.64 ($^2J_{CF} = 16.0$ Hz), 116.65, 115.71, 113.10, 43.29, 39.18, 32.29, 27.11, and 24.70; IR cm^{-1} 3438.5, 3227.7, 1677.0, 1608.6, 1551.6, 1428.1, 1250.1, 1202.9, 1138.2; LRMS-EI m/z 558 (48%, [M$^+$]), 309 (36%); HRMS-ESI calculated for C$_{31}$H$_{29}$FN$_3$O$_4$S$^+$ [M+H$^+$] 558.1857, found 558.1901.

Methyl 2-(2-(3-aminophenyl)-5-(1-(4-(1,3-dioxoisoindolin-2-yl)butyl)-3-fluoro-2-phenyl-1H-indole-6-carbonyl)thiophen-3-yl)acetate (3y). A mixture of **2** (20 mg, 0.03 mmol), Pd(PPh$_3$)$_4$ (7 mg, 0.006 mmol), CsF (13 mg, 0.09 mmol), 3-aminophenylboronic acid (6 mg, 0.04 mmol), and H$_2$O (60 μL) in 1,2-dimethoxyethane (4 mL) was degassed with N$_2$ for 10 minutes and then refluxed until all the starting ester had been consumed (3 hours). The resulting black suspension was poured into H$_2$O (10 mL) and then extracted with 40 mL Et$_2$O. The organic layer was washed with brine (2×20 mL), dried over MgSO$_4$, and then concentrated *in vacuo*. MPLC purification (Hex:EtOAc/5:1) of the residue gave **3y** as a yellow solid foam (15 mg, 74%). ^{1}H NMR (CDCl$_3$) δ 7.99 (s, 1H), 7.78−7.76 (m, 2H), 7.71−7.67 (m, 5H), 7.51−7.37 (m, 5H), 7.24 (t, $J = 7.6$ Hz, 1H), 6.88 (d, $J = 7.2$ Hz, 1H), 6.83 (s, 1H), 6.73 (d, $J = 7.2$ Hz, 1H), 4.26 (t, $J = 7.0$ Hz, 2H), 3.72 (s, 2H), 3.69 (s, 3H), 3.48 (t, $J = 6.8$ Hz, 2H), 1.66−1.58 (m, 2H), and 1.50−1.45 (m, 2H) (see Figure S5 for proton NMR spectrum of **3y**); ^{13}C NMR (CDCl$_3$) δ 188.12, 171.73, 168.51, 149.72, 147.07, 141.92 ($^1J_{CF} = 245.0$ Hz), 141.74, 137.49, 134.19, 134.09, 132.46, 132.36 ($^3J_{CF} = 6.0$ Hz), 132.13, 130.36, 129.96, 129.15, 129.05, 128.58 ($^3J_{CF} = 3.0$ Hz), 127.21 ($^2J_{CF} = 10.7$ Hz), 123.46, 121.39, 119.94 ($^3J_{CF} = 6.1$ Hz), 119.71, 116.89, 115.80 ($^2J_{CF} = 15.3$ Hz), 112.59, 52.41, 43.61, 37.25, 34.50, 27.36, and 25.77; IR cm^{-1} 3456.5, 3366.6, 2945.7, 1711.7, 1601.4 and 1393.0; LRMS-EI m/z 686 (100%, [M$^+$]); HRMS-ESI calculated for C$_{40}$H$_{33}$FN$_3$O$_5$S$^+$ [M+H$^+$] 686.2119, found 686.2128.

2-(5-(1-(4-Aminobutyl)-3-fluoro-2-phenyl-1H-indole-6-car-bonyl)-2-(3-aminophenyl)thiophen-3-yl)-N-hydroxyacetamide (F3A). To a stirred solution of **3y** (15 mg, 0.022 mmol) in THF/MeOH (0.5 mL/0.5 mL), 0.5 mL of 50% aqueous NH$_2$OH was added, followed by a catalytic amount (two crystals) of KCN. The resulting mixture was stirred for 16 hours at room temperature, and then filtered through a short Celite column. HPLC purification (eluting time: 20 minutes) of the filtrate gave **F3A·2TFA** as a yellow solid foam (12 mg, 71%). The semi-preparative and analytical HPLC retention times of **F3A·2TFA** are 13.12 and 12.25 minutes, respectively (see Figure S6 for chromatograms of **F3A·2TFA** before and after the HPLC purification). ^{1}H NMR (CD$_3$OD) δ 8.12 (s, 1H), 7.82 (s, 1H), 7.74 (d, $J = 8.4$ Hz, 1H), 7.69 (d, $J = 8.4$ Hz, 1H), 7.66−7.51 (m, 8H), 7.44−7.42 (m, 1H), 4.37 (t, $J = 6.8$ Hz, 2H),

3.54 (s, 2H), 2.78 (t, $J = 7.2$ Hz, 2H), 1.76−1.68 (m, 2H), and 1.49−1.41 (m, 2H) (see Figure S7 for proton NMR spectrum of **F3A**); ^{13}C NMR (CD$_3$OD) δ 188.54, 168.75, 160.22 (q, CF$_3$$\underline{C}O_2$H, $^2J_{CF} = 39.7$ Hz), 146.93, 142.57, 141.73 ($^1J_{CF} = 243.1$ Hz), 137.34, 134.89, 134.07, 132.54, 132.20 ($^3J_{CF} = 5.4$ Hz), 131.88, 130.72, 129.86, 129.08, 128.99, 128.38 ($^3J_{CF} = 3.1$ Hz), 128.29, 127.57 ($^2J_{CF} = 20.5$ Hz), 122.62 ($^2J_{CF} = 32.0$ Hz), 120.69, 119.83 ($^2J_{CF} = 15.3$ Hz), 116.65, 116.23 (q, $\underline{C}$F$_3$CO$_2$H, $^1J_{CF} = 287.4$ Hz), 113.08, 43.28, 39.15, 32.28, 27.06, and 24.67; IR cm^{-1} 3432.0, 2925.3, 1679.0, 1200.9, 1135.5; LRMS-EI m/z 557 (60%, [M$^+$]), 309 (62%); HRMS-ESI calculated for C$_{31}$H$_{30}$FN$_4$O$_3$S$^+$ [M+H$^+$] 557.2017, found 557.2040.

in Vitro Evaluation

Assays of the BoNTAe activity were done at 37°C and contained 0.5 mM substrate, 0.5–1.5 μg/mL recombinant BoNTAe, 40 mM HEPES, 1 mM dithiothreitol, 25 μM ZnCl$_2$, 0.5 mg/mL BSA, and 0.05% tween at pH 7.3. Substrate for BoNTAe was an SNAP-25 fragment containing residues 187–203 with *N*- and *C*-termini acylated and amidated, respectively [28]. Inhibitors were dissolved in dimethyl sulfoxide at 10 times the final assay concentration, then diluted into the assay mixture containing substrate, followed by addition of the endopeptidase (*i.e.*, inhibitor and endopeptidase were not preincubated). Assay times and endopeptidase concentrations were adjusted so that less than 10% of the substrate was hydrolyzed. Assays were stopped by acidification with TFA and analyzed by reverse-phase HPLC as described previously [25].

in Vivo Evaluation

Pharmacokinetics Study. The *in vivo* pharmacokinetic parameters were determined by dosing 6 Balb/c mice intraperitoneally with a test inhibitor at 2 mg/kg at which concentration no obvious sign of toxicity was observed. Blood was collected by cardiac puncture at 0.5, 1, 2, 4, 8, and 24 hours and the plasma was separated and kept frozen at −80°C until processing. Each experiment was repeated three times. The plasma was thawed and extracted with two volumes of ice-cold acetonitrile to precipitate plasma proteins and release the inhibitor. The organic phase was analyzed by liquid chromatography mass spectrometry and the concentration of the inhibitor was determined based on a standard curve run in parallel. The stability of the inhibitor in acetonitrile was determined prior to analyzing pharmacokinetic samples. Pharmacokinetic values were determined with WinNonLin software from Pharcite based on the plasma concentration curve.

Protection Study. The protection studies were carried out by using a standardized mouse model of botulism [26]. Briefly, groups of Balb/c mice were given a single 2-mg/kg intraperitoneal injection of **H3H**, **F4H**, **F3A** or dimethyl sulfoxide as a control and, after 30 minutes, each mouse was challenged intraperitoneally with BoNTA at 5 times of its median-lethal dose. Dimethyl sulfoxide was used as a carrier vehicle because **H3H** is water insoluble. All mice were examined twice daily for survival, behaviour, motor activity, breath, and extraocular symptoms of botulism. The numbers of mice in the treated and control groups were 10 and 5, respectively. Survival curves were constructed based on the number of survivors and statistically analyzed using GraphPad Prism 5.0 (Graphpad Software, Inc.).

Computer Simulations

Model Preparation. The atomic charges of **F4H** and **F3A** were obtained according to the RESP procedure [29] with *ab initio* calculations at the HF/6-31G*//HF/6-31G* level using the

Gaussian 98 program [30]. The starting structure of inhibitor•BoNTAe was generated by (1) manually docking the inhibitor into the BoNTAe active site and (2) replacing the active-site zinc ion with the tetrahedral zinc ion using the cationic dummy atom approach [23,31–33]. In the manual docking, the hydroxamate group was placed near the tetrahedral zinc ion, the thiophene-substituted phenyl group was placed near Arg363, and the ammonium group was placed near Glu64. The BoNTAe structure used for the docking was taken from the crystal structure of an inhibitor-bound BoNTAe (Protein Data Bank Code: 3BOO [34]) whose conformations of missing residues 62–67 were taken from the crystal structure of a BoNTAe mutant in complex with SNAP-25 (Protein Data Bank Code: 1XTG [35]). For BoNTAe, His223 and His227 were treated as HIN (histidinate) [32,36,37]; His39, His230, and His269 were treated as HID; all other His residues were treated as HIP; Glu261 and Glu351 were treated as GLH [32,36,37]. A total of 111 crystallographically determined water molecules (named HOH) located inside the enzyme were included for simulations. The topology and coordinate files of the water-containing inhibitor•BoNTAe complex were generated by the PREP, LINK, EDIT, and PARM modules of the AMBER 5.0 program [38]. The complex was refined by energy minimization using a dielectric constant of 1.0 and 100 cycles of steepest-descent minimization followed by 100 cycles of conjugate-gradient minimization. The refined complex was solvated with 13,617 and 13,540 TIP3P water molecules (named WAT) [39] for **F4H** and **F3A**, leading to a system of 48,096 and 47,866 atoms, respectively. The WAT molecules were obtained from solvating the complex using a pre-equilibrated box of 216,000 TIP3P molecules, whose hydrogen atom charge was set to 0.4170, where any water molecule was removed if it had an oxygen atom closer than 2.2 Å to any solute atom or a hydrogen atom closer than 2.0 Å to any solute atom, or if it was located further than 9.0 Å along the x-, y-, or z-axis from any solute atom.

Multiple Molecular Dynamics Simulations. The solvated complex system was energy-minimized for 100 cycles of steepest-descent minimization followed by 100 cycles of conjugate-gradient minimization to remove close van der Waals contacts in the system, then heated from 0 to 300 K at a rate of 10 K/ps under constant temperature and volume, and finally simulated independently with a unique seed number for initial velocities at 300 K under constant temperature and pressure using the PMEMD module of the AMBER 8.0 program [40] with the AMBER force field (ff99SB) [41,42]. All simulations used (1) a dielectric constant of 1.0, (2) the Berendsen coupling algorithm [43], (3) a periodic boundary condition at a constant temperature of 300 K and a constant pressure of 1 atm with isotropic molecule-based scaling, (4) the Particle Mesh Ewald method to calculate long-range electrostatic interactions [44], (5) a time step of 1.0 fs, (6) the SHAKE-bond-length constraints applied to all the bonds involving the H atom, (7) saving the image closest to the middle of the "primary box" to the restart and trajectory files, (8) formatted restart file, and (9) default values of all other inputs of the PMEMD module. Ten different molecular dynamics simulations (each lasted 10 ns) were carried out for the BoNTAe in complex with **F4H** or **F3A** on a cluster of Apple Mac Pros with 80 Intel Xeon cores (3.0 GHz).

Simulation Analysis. For each of the 10 simulations of **F4H**•BoNTAe or **F3A**•BoNTAe, 100 instantaneous conformations were saved at 10-ps intervals during the last 1-ns period. A total of 1,000 instantaneous conformations of **F4H**•BoNTAe or **F3A**•BoNTAe from the 10 simulations were subjected to a cluster analysis using the averagelinkage algorithm (epsilon = 2.0 Å and RMS on alpha-carbon atoms) [45] implemented in the PTRAJ module of the AMBER 10 program [40]. Only one cluster of the BoNTAe

conformations was identified. All 1,000 instantaneous conformations of **F4H**•BoNTAe or **F3A**•BoNTAe were subjected to a second-round cluster analysis using the averagelinkage algorithm (epsilon = 1.5 Å and RMS on all atoms of **F4H or F3A**) [45]. This analysis identified 7 and 4 clusters for the **F4H** and **F3A** conformations, respectively. The numbers of the **F4H** conformations in Clusters 1–7 are 200, 100, 423, 27, 150, 30, and 70, respectively; the numbers of the **F3A** conformations in Clusters 1–4 are 600, 299, 1, and 100, respectively. The representative conformations of **F4H**•BoNTAe and **F3A**•BoNTAe from their most populated clusters overlay reasonably well (see Figure 3) and are considered as plausible complex structures in water. The coordinates of the representative conformations are available from Datasets S1 and S2. The coordinates of other conformations are available upon request.

Supporting Information

Figure S1 Proton NMR spectrum of 2.
Found at: doi:10.1371/journal.pone.0010129.s001 (0.79 MB PDF)

Figure S2 Proton NMR spectrum of 3x.
Found at: doi:10.1371/journal.pone.0010129.s002 (0.56 MB PDF)

Figure S3 Chromatograms of F4H·TFA before and after the HPLC purification.
Found at: doi:10.1371/journal.pone.0010129.s003 (0.17 MB PDF)

Figure S4 Proton NMR spectrum of F4H.
Found at: doi:10.1371/journal.pone.0010129.s004 (0.54 MB PDF)

Figure S5 Proton NMR spectrum of 3y.
Found at: doi:10.1371/journal.pone.0010129.s005 (0.50 MB PDF)

Figure S6 Chromatograms of F3A·2TFA before and after the HPLC purification.
Found at: doi:10.1371/journal.pone.0010129.s006 (0.17 MB PDF)

Figure S7 Proton NMR spectrum of F3A.
Found at: doi:10.1371/journal.pone.0010129.s007 (0.43 MB PDF)

Dataset S1 Coordinates of simulation-generated model of F4H·BoNTAe.
Found at: doi:10.1371/journal.pone.0010129.s008 (0.46 MB TXT)

Dataset S2 Coordinates of simulation-generated model of F3A·BoNTAe.
Found at: doi:10.1371/journal.pone.0010129.s009 (0.47 MB TXT)

Acknowledgments

Author Contributions

Conceived and designed the experiments: Y-PP JD JJS CBM. Design of F4H and F3A: Y-PP SW JGP. Syntheses of F4H, F3A, and H3H: SW. Performed the experiments: Y-PP JD SW JGP MPN JJS. Analyzed the data: Y-PP JD SW JGP MPN JJS CBM. Wrote the paper: Y-PP JD CBM. Contributed with revisions: Y-PP JD SW JGP MPN JJS CBM.

References

1. Shapiro RL, Hatheway C, Swerdlow DL (1998) Botulism in the United States - a clinical and epidemiologic review. Ann Intern Med 129: 221–228.
2. Kessler KR, Benecke R (1997) Botulinum toxin—from poison to remedy. Neurotoxicology 18: 761–770.
3. Springen K, Raymond J, Skipp C, Scelfo J, SS (2002) The Botox boom. Newsweek. pp 50–58.
4. Crowner BE, Brunstrom JE, Racette BA (2007) Iatrogenic botulism due to therapeutic botulinum toxin A injection in a pediatric patient. Clin Neuropharmacol 30: 310–313.
5. Kuehn BM (2009) FDA requires black box warnings on labeling for botulinum toxin products. JAMA 301: 2316.
6. Liang BA (2006) Fade to black: importation and counterfeit drugs. Am J Law Med 32: 279–323.
7. Foran PG, Mohammed N, Lisk GO, Nagwaney S, Lawrence GW, et al. (2003) Evaluation of the therapeutic usefulness of botulinum neurotoxin B, C1, E, and F compared with the long lasting type A. Basis for distinct durations of inhibition of exocytosis in central neurons. J Biol Chem 278: 1363–1371.
8. Arnon SS, Schechter R, Inglesby TV, Henderson DA, Bartlett JG, et al. (2001) Botulinum toxin as a biological weapon: medical and public health management. JAMA 285: 1059–1070.
9. Franz DR, Jahrling PB, Friedlander AM, McClain DJ, Hoover DL, et al. (1997) Clinical recognition and management of patients exposed to biological warfare agents. JAMA 278: 399–411.
10. Wein LM, Liu Y (2005) Analyzing a bioterror attack on the food supply: the case of botulinum toxin in milk. Proc Natl Acad Sci USA 102: 9984–9989.
11. Arnon SS (2007) Creation and development of the public service orphan drug Human Botulism Immune Globulin. Pediatrics 119: 785–789.
12. Larsen JC (2009) U.S. Army botulinum neurotoxin (BoNT) medical therapeutics research program: past accomplishments and future directions. Drug Develop Res 70: 266–278.
13. Boldt GE, Eubanks LM, Janda KD (2006) Identification of a botulinum neurotoxin A protease inhibitor displaying efficacy in a cellular model. Chem Commun (Camb). pp 3063–3065.
14. Tang J, Park JG, Millard CB, Schmidt JJ, Pang Y-P (2007) Computer-aided lead optimization: improved small-molecule inhibitor of the zinc endopeptidase of botulinum neurotoxin serotype A. PLoS ONE 2: e761.
15. Burnett JC, Ruthel G, Stegmann CM, Panchal RG, Nguyen TL, et al. (2007) Inhibition of metalloprotease botulinum serotype A from a pseudo-peptide binding mode to a small molecule that is active in primary neurons. J Biol Chem 282: 5004–5014.
16. Johnson SL, Chen LH, Harbach R, Sabet M, Savinov A, et al. (2008) Rhodanine derivatives as selective protease inhibitors against bacterial toxins. Chem Biol Drug Des 71: 131–139.
17. Moe ST, Thompson AB, Smith GM, Fredenburg RA, Stein RL, et al. (2009) Botulinum neurotoxin serotype A inhibitors: Small-molecule mercaptoaceta-mide analogs. Bioorg Med Chem 17: 3072–3079.
18. Roxas-Duncan V, Enyedy I, Montgomery VA, Eccard VS, Carrington MA, et al. (2009) Identification and biochemical characterization of small-molecule inhibitors of *Clostridium botulinum* neurotoxin serotype A. Antimicrob Agents Ch 53: 3478–3486.
19. Pang Y-P, Vummenthala A, Mishra RK, Park JG, Wang SH, et al. (2009) Potent new small-molecule inhibitor of botulinum neurotoxin serotype A endopeptidase developed by synthesis-based computer-aided molecular design. PLoS ONE 4: e7730.
20. Cai S, Lindo P, Park JB, Vasa K, Singh BR (2010) The identification and biochemical characterization of drug-like compounds that inhibit botulinum neurotoxin serotype A endopeptidase activity. Toxicon 55: 818–826.
21. Simpson LL (1981) The origin, structure, and pharmacological activity of botulinum toxin. Pharmacol Rev 33: 155–188.
22. Eubanks LM, Hixon MS, Jin W, Hong S, Clancy CM, et al. (2007) An *in vitro* and *in vivo* disconnect uncovered through high-throughput identification of botulinum neurotoxin A antagonists. Proc Natl Acad Sci USA 104: 2602–2607.
23. Park JG, Sill PC, Makiyi EF, Garcia-Sosa AT, Millard CB, et al. (2006) Serotype-selective, small-molecule inhibitors of the zinc endopeptidase of botulinum neurotoxin serotype A. Bioorg Med Chem 14: 395–408.
24. Muller K, Faeh C, Diederich F (2007) Fluorine in pharmaceuticals: looking beyond intuition. Science 317: 1881–1886.
25. Schmidt JJ, Bostian KA (1997) Endoproteinase activity of type A botulinum neurotoxin: substrate requirements and activation by serum albumin. J Protein Chem 16: 19–26.
26. Hatheway CH, Snyder JD, Seals JE, Edell TA, Lewis GE, Jr. (1984) Antitoxin levels in botulism patients treated with trivalent equine botulism antitoxin to toxin types A, B, and E. J Infect Dis 150: 407–412.
27. Sarvas H, Seppala I, Kurikka S, Siegberg R, Makela O (1993) Half-life of the maternal IgG1 allotype in infants. J Clin Immunol 13: 145–151.
28. Schmidt JJ, Stafford RG, Bostian KA (1998) Type A botulinum neurotoxin proteolytic activity - development of competitive inhibitors and implications for substrate specificity at the s-1' binding subsite. FEBS Lett 435: 61–64.
29. Cieplak P, Cornell WD, Bayly C, Kollman PA (1995) Application of the multimolecule and multiconformational resp methodology to biopolymers: charge derivation for DNA, RNA, and proteins. J Comput Chem 16: 1357–1377.
30. Frisch MJ, Trucks GW, Schlegel HB, Gill PMW, Johnson BG, et al. (1999) GAUSSIAN 98, Revision A.7. Gaussian, Inc Pittsburgh, PA.
31. Pang Y-P (1999) Novel zinc protein molecular dynamics simulations: steps toward antiangiogenesis for cancer treatment. J Mol Model 5: 196–202.
32. Pang Y-P, Xu K, El Yazal J, Prendergast FG (2000) Successful molecular dynamics simulation of the zinc-bound farnesyltransferase using the cationic dummy atom approach. Protein Sci 9: 1857–1865.
33. Pang Y-P (2001) Successful molecular dynamics simulation of two zinc complexes bridged by a hydroxide in phosphotriesterase using the cationic dummy atom method. Proteins 45: 183–189.
34. Silvaggi NR, Wilson D, Tzipori S, Allen KN (2008) Catalytic features of the botulinum neurotoxin A light chain revealed by high resolution structure of an inhibitory peptide complex. Biochemistry 47: 5736–5745.
35. Breidenbach MA, Brunger AT (2004) Substrate recognition strategy for botulinum neurotoxin serotype A. Nature 432: 925–929.
36. El Yazal J, Pang Y-P (1999) *Ab initio* calculations of proton dissociation energies of zinc ligands: hypothesis of imidazolate as zinc ligand in proteins. J Phys Chem B 103: 8773–8779.
37. El Yazal J, Roe RR, Pang Y-P (2000) Zinc's affect on proton transfer between imidazole and acetate predicted by *ab initio* calculations. J Phys Chem B 104: 6662–6667.
38. Pearlman DA, Case DA, Caldwell JW, Ross WS, Cheatham TE III, et al. (1995) AMBER, a package of computer programs for applying molecular mechanics, normal mode analysis, molecular dynamics and free energy calculations to simulate the structural and energetic properties of molecules. Comput Phys Commun 91: 1–41.
39. Jorgensen WL, Chandreskhar J, Madura JD, Impey RW, Klein ML (1982) Comparison of simple potential functions for simulating liquid water. J Chem Phys 79: 926–935.
40. Case DA, Cheatham TE, 3rd, Darden T, Gohlke H, Luo R, et al. (2005) The Amber biomolecular simulation programs. J Comput Chem 26: 1668–1688.
41. Hornak V, Abel R, Okur A, Strockbine B, Roitberg A, et al. (2006) Comparison of multiple Amber force fields and development of improved protein backbone parameters. Proteins 65: 712–725.
42. Wickstrom L, Okur A, Simmerling C (2009) Evaluating the performance of the ff99SB force field based on NMR scalar coupling data. Biophys J 97: 853–856.
43. Berendsen HJC, Postma JPM, van Gunsteren WF, Di Nola A, Haak JR (1984) Molecular dynamics with coupling to an external bath. J Chem Phys 81: 3684–3690.
44. Darden TA, York DM, Pedersen LG (1993) Particle Mesh Ewald: An N log(N) method for Ewald sums in large systems. J Chem Phys 98: 10089–10092.
45. Shao J, Tanner SW, Thompson N, Cheatham TE, III (2007) Clustering molecular dynamics trajectories: 1. characterizing the performance of different clustering algorithms. J Chem Theory Comput 3: 2312–2334.